

# Measurement of the CP observables in $\bar{B}_s^0 \rightarrow D_s^+ K^-$ and first observation of $\bar{B}_{(s)}^0 \rightarrow D_s^+ K^- \pi^+ \pi^-$ and $\bar{B}_s^0 \rightarrow D_{s1}(2536)^+ \pi^-$

*Steven R. Blusk*

*Department of Physics*

*Syracuse University*

*Syracuse, NY 13244, USA*

Proceedings of CKM 2012, the 7<sup>th</sup> International Workshop on the CKM Unitarity Triangle, University of Cincinnati, USA, 28th September - 2 October 2012

## 1 Introduction

A central goal of flavor physics is to measure the angle  $\gamma \equiv \arg\left(-\frac{V_{ub}^* V_{ud}}{V_{cb}^* V_{cd}}\right)$  in the Cabibbo-Kobayashi-Maskawa (CKM) [1, 2] mixing matrix, which is currently known to a precision of about 10-12° [3]. The theoretically cleanest methods employ  $B \rightarrow DK$  decays, where the sensitivity to  $\gamma$  results from the interference between  $b \rightarrow c$  and  $b \rightarrow u$  transitions. Since both transitions are  $\mathcal{O}(\lambda^3)$  in the Wolfenstein parameter [4], large CP violating asymmetries are expected. One powerful class of methods utilize  $B^- \rightarrow DK^-$  where the  $D$  is detected in either a CP eigenstate [7], a flavor-specific mode [6], or a multi-body decay [8]. An advantage of these decays is that they do not require knowledge of the  $b$ -hadron flavor at production (flavor tagging), and only rely on measuring the time integrated rates. Another powerful method to extract  $\gamma$  is to perform a time-dependent analysis of  $\bar{B}_s^0 \rightarrow D_s^+ K^-$  [9, 10, 11] and  $\bar{B}_s^0 \rightarrow D_s^+ K^- \pi^+ \pi^-$ . Time-dependent analyses of  $\bar{B}_s^0 \rightarrow D_s^+ K^- (\pi^+ \pi^-)$  are only possible at hadron colliders, and are a unique capability of LHCb.

The time-dependent decay rates of  $B_s^0$  and  $\bar{B}_s^0$  to a flavor-specific final state,

16  $f = D_s^+ K^-$ , is given by:

$$\frac{d\Gamma_{B_s^0 \rightarrow f}(t)}{dt} = \frac{1}{2}|A_f|^2(1 + |\lambda_f|^2)e^{-\Gamma_s t} \left[ \cosh\left(\frac{\Delta\Gamma_s t}{2}\right) + D_f \sinh\left(\frac{\Delta\Gamma_s t}{2}\right) + C_f \cos(\Delta m_s t) - S_f \sin(\Delta m_s t) \right] \quad (1)$$

$$\frac{d\Gamma_{\bar{B}_s^0 \rightarrow f}(t)}{dt} = \frac{1}{2}|A_f|^2 \left| \frac{p}{q} \right|^2 (1 + |\lambda_f|^2)e^{-\Gamma_s t} \left[ \cosh\left(\frac{\Delta\Gamma_s t}{2}\right) + D_f \sinh\left(\frac{\Delta\Gamma_s t}{2}\right) - C_f \cos(\Delta m_s t) + S_f \sin(\Delta m_s t) \right] \quad (2)$$

17 where  $A_f$  is the decay amplitude  $A(B_s^0 \rightarrow f)$  and  $\lambda_f = (q/p)(\bar{A}_f/A_f) = |\lambda_f|e^{i(\Delta - (\gamma - 2\beta_s))}$ .  
 18 Here,  $|\lambda_f|$  and  $\Delta$  are the relative magnitude and strong phase difference between the  
 19  $b \rightarrow u$  and  $b \rightarrow c$  transitions, and  $2\beta_s$  is the phase of  $B_s^0$  mixing. The complex coeffi-  
 20 cients  $p$  and  $q$  relate the  $B_s^0$  meson mass eigenstates,  $B_{H,L}$ , to the flavor eigenstates,  
 21  $B_s^0$  and  $\bar{B}_s^0$  via:

$$\begin{aligned} B_L &= pB_s^0 + q\bar{B}_s^0 \\ B_H &= pB_s^0 - q\bar{B}_s^0 \end{aligned}, \quad |p|^2 + |q|^2 = 1. \quad (3)$$

22 Similar equations can be written for the  $CP$ -conjugate decays, replacing  $A_f$  by  $\bar{A}_{\bar{f}} =$   
 23  $A(\bar{B}_s^0 \rightarrow \bar{f})$ ,  $\lambda_f$  by  $\bar{\lambda}_{\bar{f}} = (p/q)(A_{\bar{f}}/\bar{A}_{\bar{f}})$ ,  $|p/q|^2$  by  $|q/p|^2$ ,  $C_f$  by  $C_{\bar{f}}$ ,  $S_f$  by  $S_{\bar{f}}$ , and  $D_f$   
 24 by  $D_{\bar{f}}$ . The  $CP$  asymmetry observables  $C_f$ ,  $S_f$ ,  $D_f$ ,  $C_{\bar{f}}$ ,  $S_{\bar{f}}$  and  $D_{\bar{f}}$  are then given by

$$\begin{aligned} C_f = C_{\bar{f}} &= \frac{1 - |\lambda_f|^2}{1 + |\lambda_f|^2}, & S_f &= \frac{2\text{Im}(\lambda_f)}{1 + |\lambda_f|^2}, & D_f &= \frac{2\text{Re}(\lambda_f)}{1 + |\lambda_f|^2}, \\ S_{\bar{f}} &= \frac{2\text{Im}(\bar{\lambda}_{\bar{f}})}{1 + |\bar{\lambda}_{\bar{f}}|^2}, & D_{\bar{f}} &= \frac{2\text{Re}(\bar{\lambda}_{\bar{f}})}{1 + |\bar{\lambda}_{\bar{f}}|^2}. \end{aligned} \quad (4)$$

25 Since  $CP$  violation in mixing is expected to be below the percent level, it follows that  
 26  $|q/p| = 1$ ,  $|\lambda_f| = |\bar{\lambda}_{\bar{f}}|$ , and consequently  $C_f = C_{\bar{f}}$ . Thus there are five observables  
 27 that depend on the 3 physics parameters of interest:  $|\lambda_f|$ ,  $\Delta$  and  $\gamma - 2\beta_s$ . Similar  
 28 expressions are applicable to  $\bar{B}_s^0 \rightarrow D_s^+ K^- \pi^+ \pi^-$ , however, there is a potential dilution  
 29 due to the varying strong phase across the  $D_s^+ K^- \pi^+ \pi^-$  Dalitz plane.

30 In this article, we present the first measurements of these five  $CP$  observables.  
 31 First observations of the  $\bar{B}_s^0 \rightarrow D_s^+ K^- \pi^+ \pi^-$ ,  $\bar{B}^0 \rightarrow D_s^+ K^- \pi^+ \pi^-$  and  $\bar{B}_s \rightarrow D_{s1}(2536)^+ \pi^-$   
 32 decays are also presented, along with measurements of their relative branching frac-  
 33 tions. All results are based on  $1.0 \text{ fb}^{-1}$  of integrated luminosity recorded in 2011  
 34 by the LHCb experiment. More detailed documentation of the  $\bar{B}_s^0 \rightarrow D_s^+ K^-$  and  
 35  $\bar{B}_{(s)}^0 \rightarrow D_s^+ K^- \pi^+ \pi^-$  analyses can be found in Refs. [12] and [13], respectively.

## 2 Event Selection

Signal  $D_s^+$  candidates are formed by reconstructing  $D_s^+ \rightarrow K^+ K^- \pi^+$ ,  $D_s^+ \rightarrow \pi^+ \pi^- \pi^+$  and  $D_s^+ \rightarrow K^+ \pi^- \pi^+$ . For the  $\bar{B}_{(s)}^0 \rightarrow D_s^+ K^- \pi^+ \pi^-$  and  $\bar{B}_s^0 \rightarrow D_s^+ \pi^- \pi^+ \pi^-$  candidates, only the  $D_s^+ \rightarrow K^+ K^- \pi^+$  decay is considered. The  $D_s^+$  candidates are required to form a good quality vertex, be spacially well separated from any primary vertex (PV), and have an invariant mass consistent with the known  $D_s^+$  mass (within about 3 times the mass resolution). Multivariate selection algorithms are employed to suppress the combinatorial background, and typically have a signal efficiency of 80-90% while rejecting about 85% of the combinatorial background. Invariant mass distributions for  $D_s^+$  candidates are shown in Fig. 1 for the higher signal yield  $\bar{B}_s^0 \rightarrow D_s^+ \pi^-$  decay, showing that clean signals are achievable even in the suppressed  $D_s^+$  decay modes. Tighter

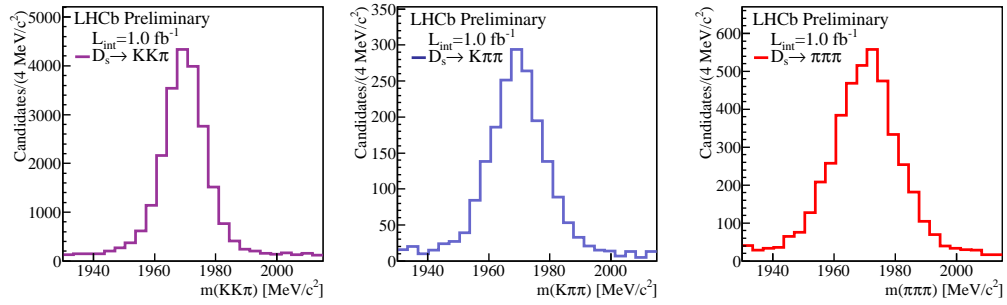


Figure 1: Invariant mass distributions for  $D_s^+$  candidates in the  $\bar{B}_s^0 \rightarrow D_s^+ \pi^-$  data sample, for (left)  $K^+ K^- \pi^+$ , (middle)  $K^+ \pi^- \pi^+$ , and (right)  $\pi^+ \pi^- \pi^+$  final states.

particle identification requirements are applied to the  $K^-$  or  $K^- \pi^+ \pi^-$  recoiling from the  $D_s^+$  to suppress cross-feed from the favored  $\bar{B}_s^0 \rightarrow D_s^+ \pi^-$  and  $\bar{B}_s^0 \rightarrow D_s^+ \pi^- \pi^+ \pi^-$  decays. For the  $\bar{B}_s^0 \rightarrow D_s^+ \pi^- \pi^+ \pi^-$  and  $\bar{B}_s^0 \rightarrow D_s^+ K^- \pi^+ \pi^-$  decays, the invariant mass of the  $\pi^- \pi^+ \pi^-$  and  $K^- \pi^+ \pi^-$  systems are restricted to be below 3000  $\text{MeV}/c^2$ .

## 3 Analysis of $\bar{B}_s^0 \rightarrow D_s^+ \pi^-$ and $\bar{B}_s^0 \rightarrow D_s^+ K^-$

The invariant mass distributions for  $\bar{B}_s^0 \rightarrow D_s^+ \pi^-$  and  $\bar{B}_s^0 \rightarrow D_s^+ K^-$  are shown in Figs. 2 and 3. All three  $D_s^+$  decay modes have approximately equal  $B_s^0$  mass resolutions, and are summed together in these distributions. The signal shape is modeled as the sum of two Crystal Ball [14] functions, with one exponential tail on each side of the  $\bar{B}_s^0$  signal peak. A number of specific backgrounds, due to either a missed particle (e.g.  $\bar{B}_s^0 \rightarrow D_s^+ \rho^-$ , with the  $\pi^0$  undetected), a misidentified particle (e.g.  $\bar{B}_s^0 \rightarrow D_s^+ \pi^-$  reconstructed as  $\bar{B}_s^0 \rightarrow D_s^+ K^-$ ), or both (e.g.  $\bar{B}_s^0 \rightarrow D_s^+ \rho^-$

reconstructed as  $\bar{B}_s^0 \rightarrow D_s^+ K^-$ ) are accounted for using either data or simulation to model the shape of these backgrounds. From an unbinned extended maximum likelihood fit,  $27,965 \pm 395$   $\bar{B}_s^0 \rightarrow D_s^+ \pi^-$  and  $1390 \pm 98$   $\bar{B}_s^0 \rightarrow D_s^+ K^-$  signal events are selected. The CP parameters are obtained by a fit to the decay time distribution

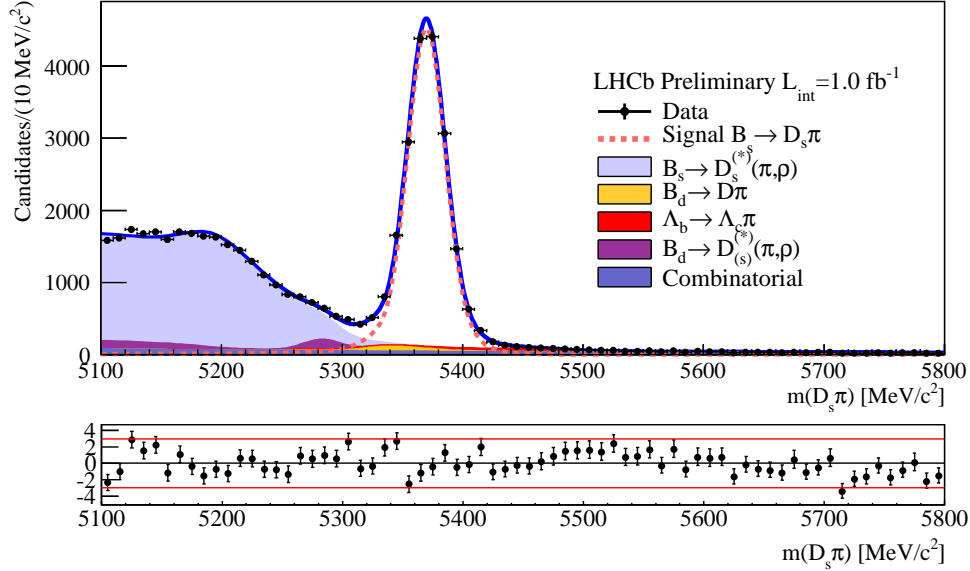


Figure 2: Invariant mass distributions  $\bar{B}_s^0 \rightarrow D_s^+ \pi^-$  candidates. The signal component is indicated by the dashed curve, and the backgrounds are indicated by the various color-filled (shaded, in B/W) curves.

of the  $\bar{B}_s^0 \rightarrow D_s^+ K^-$  signal candidates. Two methods have been developed. The first, referred to as *sFit*, uses *sWeights* [15] obtained from the  $\bar{B}_s^0 \rightarrow D_s^+ K^-$  mass fit to statistically subtract the background contribution. The second method, referred to as *cFit*, is a conventional two-dimensional fit to the reconstructed mass and decay time. The advantage of the first method is that there is no need to model the time distribution of all the backgrounds, as they are statistically removed via the *sWeights*. The statistical subtraction, as presented here, uses events in the full mass fit region, and the subtraction of this background leads to a larger statistical uncertainty than if just a narrow signal region is used. For this reason, the second method is expected to give a smaller statistical uncertainty; however it requires an accurate model of the time distributions of the backgrounds that enter into the signal region. For the analysis presented here, the *sFit* provides the nominal result, and the *cFit* is used as a cross-check.

The measurement of the CP parameters in  $\bar{B}_s^0 \rightarrow D_s^+ K^-$  requires a fit to the time-dependent decay rates. The fit accounts for (i) the acceptance versus reconstructed decay time, (ii) the decay time resolution, and (iii) the effective tagging efficiency. The

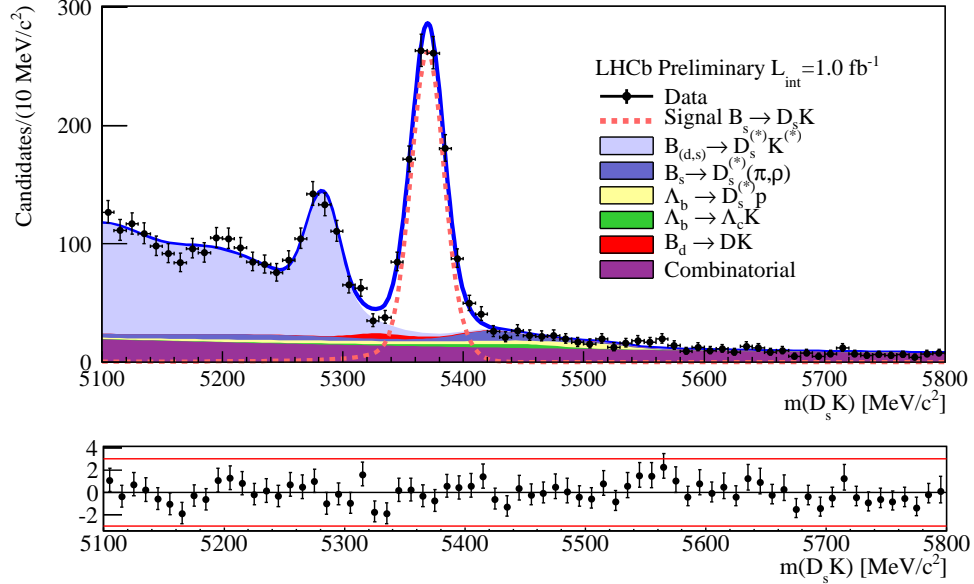


Figure 3: Invariant mass distributions  $\bar{B}_s^0 \rightarrow D_s^+ K^-$  candidates. The signal component is indicated by the dashed curve, and the backgrounds are indicated by the various color-filled (shaded, in B/W) curves.

functional form of the acceptance function is determined from simulated  $\bar{B}_s^0 \rightarrow D_s^+ \pi^-$ , and its parameters are determined in a fit to  $\bar{B}_s^0 \rightarrow D_s^+ \pi^-$  data, where the  $B_s^0$  lifetime and mixing frequency,  $\Delta m_s$ , are fixed to 1.51 ps and 17.69 ps<sup>-1</sup> [17], respectively. The average decay time resolution is about 50 fs, and is modeled by the sum of three Gaussian functions, whose parameters are determined from simulation. The Gaussian width parameters obtained from simulation are scaled up by 1.15 to account for better resolution in the simulation than in data; this factor is determined by comparing the width of the zero decay time component of prompt  $D_s^+$  plus one random track in data and simulation. For the flavor tagging, only *opposite side* (OS) taggers are currently used. These algorithms exploit the correlation in flavor between the signal  $b$  hadron at production, and the other  $b$  hadron in the event (referred to as the tag- $b$ ). In particular, the charge of either an electron, a muon, or a kaon that does not come from any  $pp$  interaction vertex (or the signal  $b$ ), or the charge of another secondary vertex in the event, provide information on the flavor of the tag- $b$  hadron. Because  $b\bar{b}$  are produced in pairs, this translates into a flavor determination of the signal  $B_s^0$ . The OS flavor tagging algorithm was initially tuned using simulated decays, and then re-optimized and calibrated to obtain the largest effective tagging efficiency using the self-tagging  $B^+ \rightarrow J/\psi K^+$  and  $B^0 \rightarrow D^{*-} \mu^+ \nu$  decays in data. In general, the performance of the OS tagging algorithms are independent of the signal  $b$ -hadron decay, and have a combined effective tagging efficiency of  $\epsilon D^2 = 1.90\%$  for

$\bar{B}_s^0 \rightarrow D_s^+ K^-$ . Further details of the tagging algorithms can be found in Ref [16].  
 In the fit to  $\bar{B}_s^0 \rightarrow D_s^+ K^-$ , the following parameters are fixed:  $\Delta m_s = 17.69 \text{ ps}^{-1}$ ,  
 $\tau_{B_s} = 1.51 \text{ ps}$  and  $\Delta\Gamma_s \equiv \Gamma_{s,L} - \Gamma_{s,H} = 0.105 \text{ ps}^{-1}$  [17]. About 60% of the  
 $\bar{B}_s^0 \rightarrow D_s^+ K^-$  candidates have no flavor tag; the time-dependent decay rates for  
 these untagged decays is given by the sum of the two expressions in Eq. 3, and  
 the sensitivity to  $\gamma$  enters through the hyperbolic sine term. The decay time distri-  
 bution of  $\bar{B}_s^0 \rightarrow D_s^+ K^-$  signal decays and projections of the fitted are shown in  
 Fig. 4. The projections show the four possible tagged decays,  $B_s^0 \rightarrow D_s^\pm K^\mp$  and  
 $\bar{B}_s^0 \rightarrow D_s^\pm K^\mp$ , as well as the untagged time-dependent decay rates ( $B_s^0, \bar{B}_s^0$ )  $\rightarrow D_s^- K^+$   
 and ( $B_s^0, \bar{B}_s^0$ )  $\rightarrow D_s^+ K^-$ . The fitted values for the CP parameters are

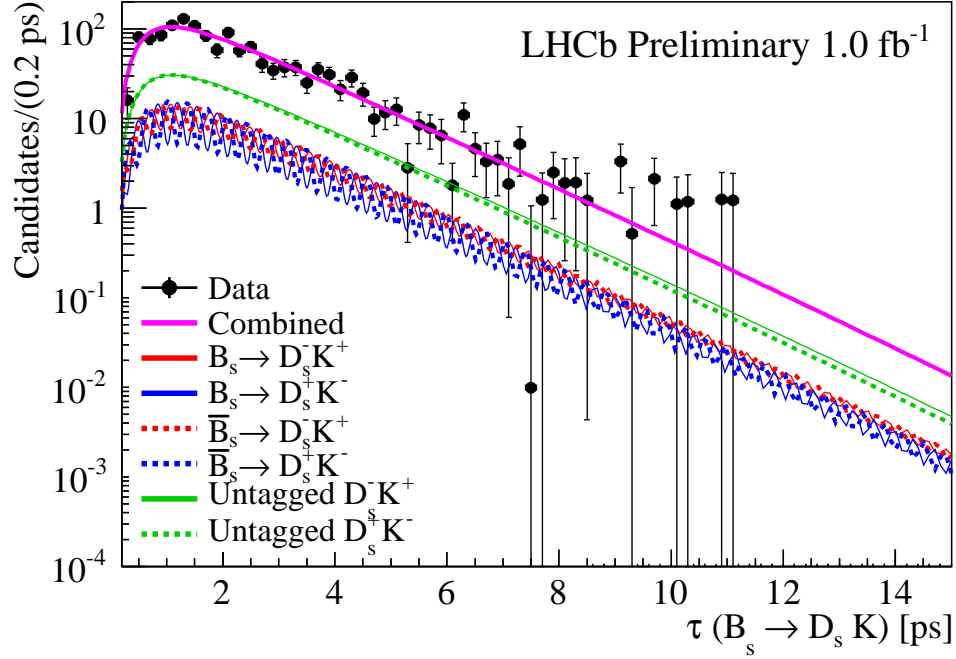


Figure 4: Distribution of reconstruct decay time for  $\bar{B}_s^0 \rightarrow D_s^+ K^-$  signal decays (points with error bars), along with the results of the fit. Projections of the decay rates versus the decay time for the four possible flavor tagged decays, and the two untagged decays.

$$\begin{aligned}
C &= 1.01 \pm 0.50 \pm 0.23, \\
S_f &= -1.25 \pm 0.56 \pm 0.24, \\
S_{\bar{f}} &= 0.08 \pm 0.68 \pm 0.28, \\
D_f &= -1.33 \pm 0.60 \pm 0.26, \\
D_{\bar{f}} &= -0.81 \pm 0.56 \pm 0.26,
\end{aligned}$$

where the first uncertainties are statistical and the second are systematic. Several sources of systematic uncertainty have been considered. The dominant sources are due to the precision on the effective flavor tagging efficiency ( $0.16\sigma_{\text{stat}}\text{--}0.23\sigma_{\text{stat}}$ ), variations in the parameters that are fixed in the default fits ( $0.15\sigma_{\text{stat}}\text{--}0.42\sigma_{\text{stat}}$ ), and the correlation between the mass of specific backgrounds and their reconstructed decay time ( $0.08\sigma_{\text{stat}}\text{--}0.27\sigma_{\text{stat}}$ ), where these uncertainties are expressed as a fraction of the statistical error. These are the first measurements of the CP parameters in  $\bar{B}_s^0 \rightarrow D_s^+ K^-$ . With additional data and analysis refinements, reduction in both the statistical and systematic uncertainties are expected.

## 4 First observation of $\bar{B}_s \rightarrow D_s^+ K^- \pi^+ \pi^-$ and $\bar{B}_s^0 \rightarrow D_{s1}(2536)^+ \pi^-$

The decay  $\bar{B}_s^0 \rightarrow D_s^+ K^- \pi^+ \pi^-$  can be analyzed in a similar way to  $\bar{B}_s^0 \rightarrow D_s^+ K^-$  to measure the weak phase  $\gamma$ . While this decay has not yet been observed, if one uses  $\bar{B}^0$  and  $B^-$  decays as a guide, it would naively be expected that its branching fraction is 1.5-2.0 times larger than  $\bar{B}_s^0 \rightarrow D_s^+ K^-$ , making this a potentially attractive decay mode to explore. The first step in such an analysis is to firmly establish an observation of this decay and measure its branching fraction (here, relative to  $\bar{B}_s^0 \rightarrow D_s^+ \pi^- \pi^+ \pi^-$ ). While searching for this decay, the decay  $\bar{B}_s^0 \rightarrow D_s^+ K^- \pi^+ \pi^-$  is also observed and its branching fraction is measured relative to  $\bar{B}_s^0 \rightarrow D_s^+ K^- \pi^+ \pi^-$ .

With the previously defined selections, Fig. 5 shows the invariant mass distributions for (left)  $\bar{B}_s^0 \rightarrow D_s^+ \pi^- \pi^+ \pi^-$  candidates and (right)  $\bar{B}_{(s)}^0 \rightarrow D_s^+ K^- \pi^+ \pi^-$  candidates. Significant  $\bar{B}_s^0$  signals are seen in both spectra, and a  $\bar{B}^0$  signal is seen in the  $D_s^+ K^- \pi^+ \pi^-$  mass distribution. The main sources of background are  $\bar{B}_s^0 \rightarrow D_s^{*+} \pi^- \pi^+ \pi^-$  (to  $\bar{B}_s^0 \rightarrow D_s^+ \pi^- \pi^+ \pi^-$ ), and  $\bar{B}_s^0 \rightarrow D_s^+ \pi^- \pi^+ \pi^-$ ,  $\bar{B}_{(s)}^0 \rightarrow D_s^{*+} \pi^- \pi^+ \pi^-$ , and  $\bar{B}_{(s)}^0 \rightarrow D_s^{*+} K^- \pi^+ \pi^-$  (to  $\bar{B}_{(s)}^0 \rightarrow D_s^+ K^- \pi^+ \pi^-$ ). Their shapes are taken from simulation, with parameters that are allowed to vary within their uncertainties. Yields of  $5683 \pm 83$   $\bar{B}_s^0 \rightarrow D_s^+ \pi^- \pi^+ \pi^-$ ,  $216 \pm 21$   $\bar{B}_s^0 \rightarrow D_s^+ K^- \pi^+ \pi^-$  and  $402 \pm 33$   $\bar{B}^0 \rightarrow D_s^+ K^- \pi^+ \pi^-$  are observed. After correcting for the relative efficiencies, the ratio

137 of branching fractions are measured to be

$$\frac{\mathcal{B}(\bar{B}_s^0 \rightarrow D_s^+ K^- \pi^+ \pi^-)}{\mathcal{B}(\bar{B}_s^0 \rightarrow D_s^+ \pi^- \pi^+ \pi^-)} = (5.2 \pm 0.5 \pm 0.3) \times 10^{-2}$$

$$\frac{\mathcal{B}(\bar{B}^0 \rightarrow D_s^+ K^- \pi^+ \pi^-)}{\mathcal{B}(\bar{B}_s^0 \rightarrow D_s^+ K^- \pi^+ \pi^-)} = 0.54 \pm 0.07 \pm 0.07,$$

where the uncertainties are statistical and systematic, respectively. These are the

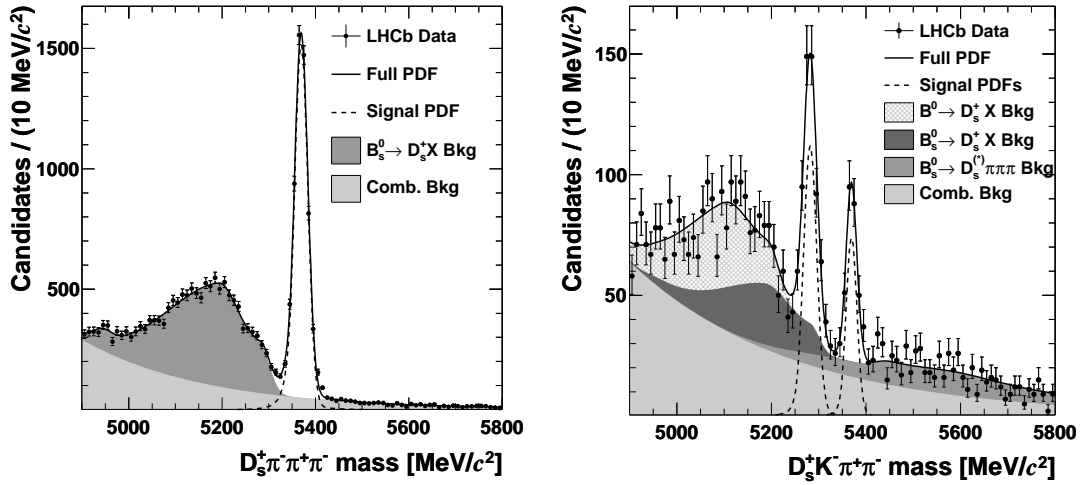


Figure 5: Invariant mass distribution for (left)  $\bar{B}_s^0 \rightarrow D_s^+ \pi^- \pi^+ \pi^-$  candidates and (right)  $\bar{B}_{(s)}^0 \rightarrow D_s^+ K^- \pi^+ \pi^-$  candidates. The fitted signal (dashed lines) and background shapes (shaded/hatched regions) are shown, as described in the text.

138

139 first observations of these decays. Since  $\bar{B}_s^0 \rightarrow D_s^+ \pi^- \pi^+ \pi^-$  has a branching fraction  
140 that is about twice as large as  $\bar{B}_s^0 \rightarrow D_s^+ \pi^-$ , and  $\mathcal{B}(\bar{B}_s^0 \rightarrow D_s^+ K^-) \sim 0.09 \times \mathcal{B}(\bar{B}_s^0 \rightarrow$   
141  $D_s^+ \pi^-)$  [18], it follows that  $\mathcal{B}(\bar{B}_s^0 \rightarrow D_s^+ \pi^- \pi^+ \pi^-)$  is at least as large as  $\mathcal{B}(\bar{B}_s^0 \rightarrow$   
142  $D_s^+ \pi^-)$ , or as much as 50% larger. The  $\mathcal{B}(\bar{B}^0 \rightarrow D_s^+ K^- \pi^+ \pi^-)$  is also sizeable, and is  
143 likely dominated by contributions where an extra  $s\bar{s}$  pair is produced in addition to  
144 the weak decay (see Ref. [13] for more details).

145 The  $\bar{B}_s^0 \rightarrow D_s^+ \pi^- \pi^+ \pi^-$  decay has also been analyzed to search for intermediate  
146 excited  $D_{sj}$  states. For  $\bar{B}_s^0 \rightarrow D_s^+ \pi^- \pi^+ \pi^-$  candidates within 40  $\text{MeV}/c^2$  of the  $\bar{B}_s^0$   
147 signal peak, the mass difference,  $\Delta M \equiv M(D_s^+ \pi^- \pi^+) - M(D_s^+)$  is computed for both  
148  $\pi^- \pi^+$  mass combinations. The resulting mass difference spectrum is shown in Fig. 6.  
149 The signal is fit with a Breit-Wigner convolved with a Gaussian resolution function



150 whose width is fixed to the expected  $\Delta M$  resolution. A signal of  $20.0 \pm 5.1$  events is  
 151 observed with a  $\Delta M$  value and width consistent with the  $D_{s1}(2536)^+$  state. Applying  
 152 corrections for the relative efficiency, the ratio of branching fractions is measured to  
 153 be

$$\frac{\mathcal{B}(\bar{B}_s^0 \rightarrow D_{s1}(2536)^+ \pi^-, D_{s1}^+ \rightarrow D_s^+ \pi^- \pi^+)}{\mathcal{B}(\bar{B}_s^0 \rightarrow D_s^+ \pi^- \pi^+ \pi^-)} = (4.0 \pm 1.0 \pm 0.4) \times 10^{-3}.$$

154 The excess of events is 5.9 standard deviations over the expected background, thus  
 establishing the first observation of this decay.

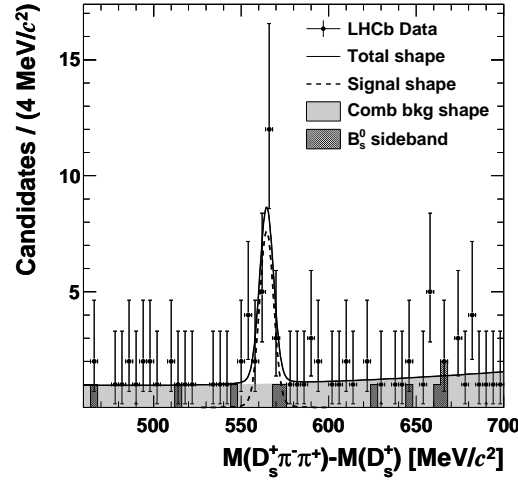


Figure 6: Distribution of the difference in invariant mass,  $M(D_s^+ \pi^- \pi^+) - M(D_s^+)$ , using  $\bar{B}_s^0 \rightarrow D_s^+ \pi^- \pi^+ \pi^-$  candidates within 40 MeV/ $c^2$  of the known  $B_s^0$  mass (points) and in the upper  $B_s^0$  mass sidebands (filled histogram). The fit to the distribution is shown, as described in the text.

155

## 156 5 Summary

157 First measurements of the CP observables in the  $\bar{B}_s^0 \rightarrow D_s^+ K^-$  decay have been re-  
 158 ported. With the larger data sample recorded in 2012, and the larger data set antici-  
 159 pated in the future, this decay will contribute significantly to the determination of the  
 160 weak phase  $\gamma$ . First observations of the  $\bar{B}_s^0 \rightarrow D_s^+ K^- \pi^+ \pi^-$  and  $\bar{B}^0 \rightarrow D_s^+ K^- \pi^+ \pi^-$   
 161 are also reported. The former can be used in a similar way to  $\bar{B}_s^0 \rightarrow D_s^+ K^-$  to

162 extract  $\gamma$ . After including  $D_s^+ \rightarrow \pi^+\pi^-\pi^+$  and  $D_s^+ \rightarrow K^-\pi^+\pi^-$  decays, and re-  
 163 optimizing the selection for  $\bar{B}_s^0 \rightarrow D_s^+K^-\pi^+\pi^-$  only, the yield in this mode more  
 164 than doubles with a comparable signal-to-background. The yield in this mode is  
 165 therefore expected to have about 35-40% of that obtained in  $\bar{B}_s^0 \rightarrow D_s^+K^-$ . The  
 166  $\bar{B}_s^0 \rightarrow D_{s1}(2536)^+\pi^-$  decay is also observed for the first time, and its branching frac-  
 167 tion relative to  $\bar{B}_s^0 \rightarrow D_s^+\pi^-\pi^+\pi^-$  is presented.

## 168 Acknowledgements

169 I gratefully acknowledge support from the National Science Foundation, which makes  
 170 this research possible.

## 171 References

- 172 [1] N. Cabibbo, Phys. Rev. Lett. **10**, 531 (1963).
- 173 [2] M. Kobayashi and T. Maskawa, Prog. Theor. Phys. **49**, 652 (1973).
- 174 [3] See talks by G. Eigen and D. Derkach in these proceedings; Also, see S. Descotes-  
 175 Genon *et al.* (CKMFitter collaboration), Proceedings Supplements, Capri, Italy,  
 176 July 11-13, 2012, to be published in Nucl. Phys. **B**. Updated results and plots  
 177 available at: <http://ckmfitter.in2p3.fr>; Also, M. Bona (UTFit collaboration),  
 178 Proceedings Supplements, Capri, Italy, July 11-13, 2012, to be published in  
 179 Nucl. Phys. **B**, with updated results at <http://www.utfit.org/UTFit>.
- 180 [4] L. Wolfenstein, Phys. Rev. Lett. **51**, 1945 (1983).
- 181 [5] See contributions by S. Malde and M. John, these proceedings.
- 182 [6] D. Atwood, G. Eilam, M. Gronau, and A. Soni, Phys. Lett. **B341**, 372 (1995).
- 183 [7] M. Gronau and D. London, Phys. Lett. **B253**, 483 (1991); M. Gronau and  
 184 D. Wyler, Phys. Lett. **B265**, 172 (1991).
- 185 [8] A. Giri, Y. Grossman, A. Soffer, and J. Zupan, Phys. Rev. **D68**, 054018 (2003).
- 186 [9] R. Aleksan, I. Dunietz and B. Kayser, Z. Phys. **C54**, 653 (1992).
- 187 [10] R. Fleischer, Nucl. Phys. **B671**, 459 (2003).
- 188 [11] K. De Bruyn, R. Fleischer, R. Knegjens, M. Merk, M. Schiller and N. Tuning,  
 189 Nucl. Phys. **B868**, 351 (2012).
- 190 [12] LHCb collaboration, LHCb-CONF-2012-029.

- 191 [13] R. Aaij (LHCb collaboration), LHCb-PAPER-2012-033, arXiv:1211.1541, sub-  
192 mitted to Phys. Rev. **D**.
- 193 [14] T. Skwarnicki, PhD thesis, Institute of Nuclear Physics, Krakow, 1986, DESY-  
194 F31-86-02.
- 195 [15] M. Pivk and F. R. Le Diberder, Nucl. Instrum. Meth. **A555**, 356 (2005).
- 196 [16] R. Aaij et. al. (LHCb Collaboration), Eur. Phys. J. **C72**, 2022 (2012); LHCb-  
197 CONF-2012-026; Also see contribution by J. Wishahi in these proceedings.
- 198 [17] Heavy Flavor Averaging Group, D. Asner et al., Averages of b-hadron,  
199 chadron, and tau-lepton Properties, arXiv:1010.1589, Online updates available  
200 at <http://www.slac.stanford.edu/xorg/hfag/>.
- 201 [18] Particle Data Group, J. Beringer *et al.*, Phys. Rev. **D86**, 010001 (2012).